Geomechanics and Engineering, *Vol. 35, No. 2 (2023) 165-179*
https://doi.org/10.12989/gae.2023.35.2.165

Uplift capacity of single vertical belled pile embedded at shallow depth

Jung-goo Kang[1a], Young-sang Kim[2b] and Gyeongo Kang*[1]

[1]*Department of Civil Engineering, Gwangju University, 277 Hyodeck-ro, Nam-gu, Gwangju, 61743, Republic of Korea*
[2]*Department of Civil Engineering, Chonnam National University, 77 Yongbong-ro, Buk-gu, Gwangju, 61186, Republic of Korea*

(*Received November 14, 2022, Revised August 29, 2023, Accepted August 30, 2023*)

Abstract. This study investigates the uplift capacity of a single vertical belled pile buried at shallow depth in dry sand. The laboratory model experiments are conducted with different pile-tip angles and relative densities. In addition, image and FEM analyses are performed to observe the failure surface of the belled pile for different pile-tip angles and relative densities. Accordingly, the uplift capacity and failure angle in the failure surface of the belled pile were found to depend on the belled pile-tip angle and relative density. A predictive model for the uplift capacity of the belled pile was proposed considering the relative density and belled pile-tip angle based on a previous limit equilibrium equation. To validate the applicability of the proposed model, the values calculated using the proposed and previous models were compared to those obtained through a laboratory model experiment. The proposed model had the best agreement with the laboratory model experiment.

Keywords: belled pile; FEM analysis; image analysis; model experiment;shallow depth; uplift capacity

1. Introduction

Frequent natural disasters, such as typhoons, tsunamis, floods, and earthquakes, impose horizontal loads (external forces) on structures. The generated external forces damage the structure due to overturning and collapse. Therefore, the structure foundation subjected to high horizontal loads (e.g., high chimneys, coastal structures, and wind power generators) requires high stability, and uplift and bearing capacities.

A belled pile, which is constructed by expanding the pile tip, is often used to improve the ground uplift capacity. Moreover, it has higher tip-bearing and uplift capacities than a conventional pile owing to its expanded pile tip. Therefore, it is very effective for achieving the ultimate uplift capacity because of the effects of frictional force and the anchor plate, which are attributable to the expanded pile tip. However, the uplift capacity mechanism of the belled pile has not been fully investigated, and, consequently, its design methodology has not yet been clarified. In addition, classifying foundations according to the embedment ratio is ambiguous owing to the change in slenderness ratio resulting from the belled pile-tip diameter being 2–3 times larger than that of a conventional pile. Therefore, the belled pile design standard is dependent on the belled pile-tip dimension, which is problematic.

*Corresponding author, Professor
E-mail: gokang@gwangju.ac.kr
[a]Ph.D.
E-mail: cocoya0305@gmail.com
[b]Professor
E-mail: geoyskim@jnu.ac.kr

Conventional and belled piles and anchor plates have been primarily studied via laboratory models and large-scale field experiments (Majer 1955, Balla 1961, Downs and Chieurzzi 1966, Matsuo 1967, 1968, Khadilkar *et al.* 1971, Clemence and Veesaert 1977, Chattopadhyay and Pise 1986, Ghaly *et al.* 1991, Ilamparuthi and Muthukrishnaiah 1999). Dickin and Leung (1990, 1992) performed a few centrifugal model tests to investigate the effect of the uplift capacity of a belled pier in sandy ground on the failure surface. They observed that the uplift capacity of a belled pier significantly depends on the embedment ratio of the pier and sand density. In addition, the effects of shaft/bell diameter ratio and bell angle in the design of a belled pier should be considered. Tsutsui *et al.* (1995) conducted field experiments on a belled pile to validate the behavior of the uplift capacity obtained from a previous laboratory model test. Based on the results, they proposed an empirical formula to predict the belled pile uplift capacity. Chatani *et al.* (2008) estimated the lowest pile skin frictional force in belled piles via axial tensile load tests and proposed its use for design. However, this method tends to underestimate the belled pile uplift capacity. Qian *et al.* (2019, 2020) conducted large-scale laboratory model and field tests for a conventional pile and belled pier considering various conditions, such as ground slope, static load, horizontal load, and lateral load. The belled pier exhibited a higher bearing capacity than a conventional pile under lateral and uplift loads. In addition, the uplift capacity of the belled pier was high in different soil conditions, including clay, gravel, and frozen soil.

Several researchers have proposed predictive models for uplift capacity based on various laboratory and field experiments on belled piles. Most proposed predictive models for the uplift capacity comprised the pile weight, shear force of the failure surface, and weight of the soil

ISSN: 2005-307X (Print), 2092-6219 (Online)

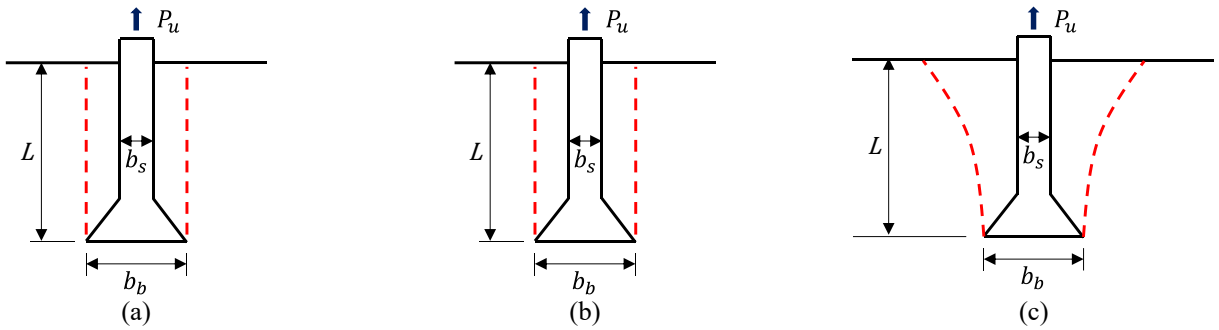

Fig. 1 Representative failure surface models for a conventional pile, anchor plate, screw pile, and belled pile: (a) vertical slip surface model, (b) inverted truncated-cone model, and (c) curved slip surface model (Date from Dickin and Leung 1990)

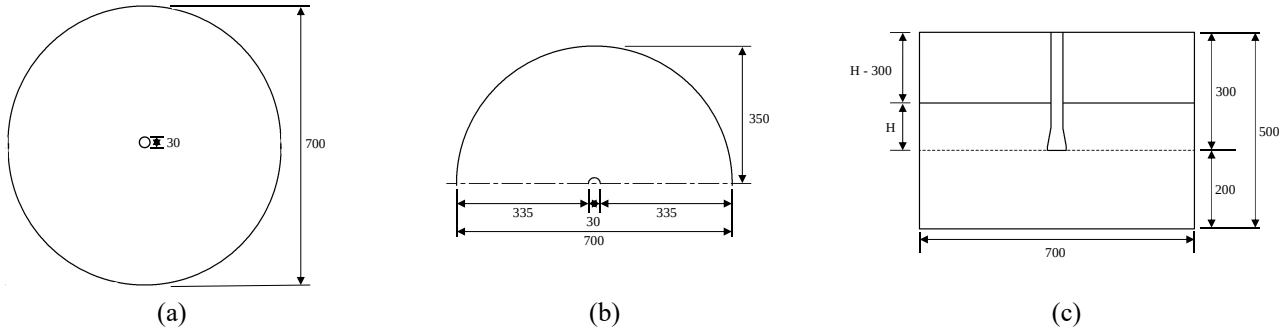

Fig. 2 Schematic diagrams of circular and half-circular chambers: (a) plan view of circular chamber, (b) plan view of half-circular chamber, and (c) front view of chamber

inside the failure surface. Here, the weight of the pile can be easily determined, but identifying the failure surface and determining the resistance (pile–soil friction) at the failure surface are challenging because of their susceptibility to factors such as ground conditions, pile shape, and penetration ratio. Therefore, researchers have verified the failure surface mechanisms of a belled pile through laboratory experiments, and they then proposed several models for predicting its uplift capacity (Dickin and Leung 1990, Honda *et al.* 2011, Niroumand *et al*. 2013, Keskin *et al.* 2015, Nazir *et al.* 2015, Emirler *et al.* 2016, Deb and Pal 2019a, b, Wang *et al.* 2020, Schafer and Madabhushi. 2020). Fig. 1 shows representative failure surface models for a conventional pile, anchor plate, screw pile, and belled pile. The proposed failure surface models can be classified into the 1) vertical slip surface model, 2) inverted truncated-cone model, and 3) curved slip surface model (Majer 1955, Balla 1961, Downs and Chieurzzi 1966, Clemence and Veesaert 1977, Murray and Geddes 1987, Meyerhof and Adams. 1968). The shape of the failure surface depends on factors such as the penetration ratio, slope condition of the ground, and belled pile-tip angle. Moreover, the shear stress at the failure surface can be calculated from the internal friction angle, adhesive force, relative density, and water content according to the ground conditions, among others. However, most previous studies focused on belled piles buried in deep foundations. Thus, the research results cannot meet all the field conditions and are unsuitable for belled piles constructed for shallow-depth applications. The belled pier or belled pile with an expanded pile tip is mainly applied to a single pile foundation for power transmission towers, bridge piers, and housing and is buried at shallow depths. However, despite its practical value, belled piles at shallow depth have not been sufficiently studied.

This study focuses on examining the uplift capacity of a belled pile buried at a shallow depth. A series of laboratory model experiments are conducted considering the effects of the belled pile-tip angle and relative density of sand. In addition, image and finite element method (FEM) analyses were used to verify the shape of the failure surface obtained from the model experiment. Finally, a predictive model for the uplift capacity of the belled pile buried at a shallow depth was proposed based on the results. The proposed predictive model was compared to previous predictive models to validate the former.

2. Material and methods

2.1 Model chambers and model piles

Circular chamber and half-circular chamber models were used in the model tests. The circular chamber was primarily used for conducting the static tension uplift load tests. In contrast, the half-circular chamber was primarily used to observe the failure behavior and interaction between the belled pile and sand through image analysis. Fig. 2 shows schematics of the circular and half-circular chambers: their heights and diameters are 500 mm and 750 mm, respectively.

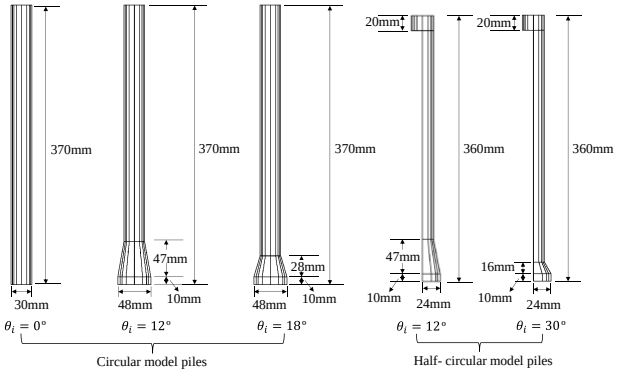

Fig. 3 Model piles: circular model piles (θ_i = 0° 12° and = 18°) and half-circular model piles (θ_i = 12° and 30°)

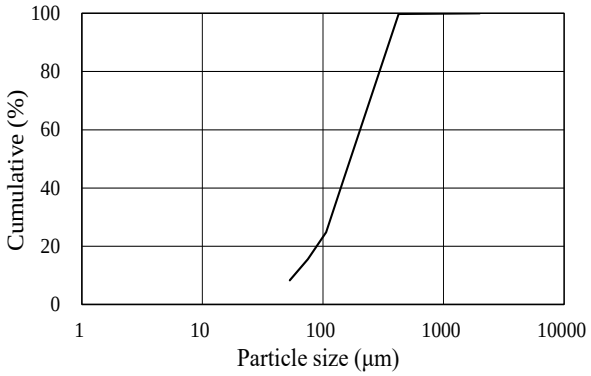

Fig. 4 Particle size distribution curve of Kumamoto silica sand (K7)

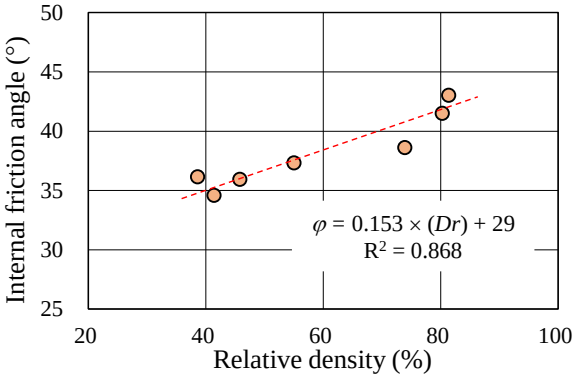

Fig. 5 Relationship between the relative density (Dr) and internal friction angle (φ)

Laboratory model tests using the model chamber require that the confinement effect of the chamber wall for the limited model ground size be considered. Therefore, the scale effect and boundary conditions of the model chamber in this study were based on the results of previous studies on conventional piles and anchor plates (Kishida 1963, Robinsky and Morrison 1964, Dash and Pise 2003). In the latter, the range of ground affected by the installation and load of piles depends on the unit weight, penetration depth, shaft diameter, and belled diameter among others, with effects extending up to 2–8 times the pile diameter being reported (Meyerhof 1959). In this study, the round ranges based on the shaft diameter (bs) and belled diameter (b_b) of the belled pile were 25D (25b_s) and 15.6D (15.6b_b), respectively, in agreement with previous research. Therefore, no effects of the boundary condition and scale effect caused by the side wall of the chamber owing to the chamber size are presumed.

The chamber used in the experiment was designed to increase its effectiveness. The circular chamber comprises two wall parts and a bottom part, and the half-circular chamber comprises a circular-chamber wall part, with a 1 cm front transparent chamber plate and bottom plate being assembled. The parts of the chamber wall and front transparent chamber plate were made of 3 mm steel and a 1 cm-thick acrylic plate, respectively. The bottom plate was made of a 1.5 cm steel plate to suppress deformation due to the weight of the ground material and each part. The steel wall and floor parts were coated with Teflon inside the soil to minimize friction between the soil and chamber wall.

Fig. 3 shows the model piles used in the circular-chamber and half-circular chamber models. All model piles were made of steel to minimize the deformation and friction in the smooth-surface piles. The uplift load model tests were conducted with three small-scale piles and different pile-tip angles (θ_i = 0°, 12°, and 18°) and sand relative densities (Dr = 40%, 60%, 75%, 85%, and 95%) at the circular chamber. In addition, two types of small-scale belled piles of θ_i = 12° and 30° were used in the image analysis at the half-circular chamber under relative densities of 40, 75, and 95%. The tip diameters of the straight (0°) and belled piles (12° and 18°) in the static tension uplift load test at the circular chamber were 30 mm and 48 mm, respectively. Moreover, the total length of the circular-chamber piles was 370 mm. The tip diameter and length of the belled pile (12° and 30°) at the half-circular chamber were 24 mm and 360 mm, respectively. The pile length at the half-circular chamber was 10 mm shorter than that at the circular chamber to ensure that the pile part applies the tensile load.

2.2 Test soil and sand beds

Kumamoto silica sand (K7) was used as the main ground material: its physical properties are listed in Table 1, whereas its particle size distribution is shown in Fig. 4. K7 was classified as nonplastic silty sand (SM) in the Unified Soil Classification System. The mean grain size and specific gravity were 168.4 μm and 2.63, respectively. The maximum and minimum densities were measured in accordance with JIS A 1224 (2009), and their values were 1.57 and 1.20 g/cm^3, respectively. Relative densities ranging from 38% to 81% were utilized for the direct shear test in accordance with JGS 0560 (2009) to determine the correct internal friction angle (φ) at the set relative density (Dr). Fig. 5 demonstrates the relationship between φ and Dr, based on which $\varphi = 0.153 \cdot Dr + 29$ was proposed for calculating the relative density. Accordingly, φ applied to the Dr utilized in this experiment was calculated using the proposed equation.

The relative density of the sand beds used in this study can be divided into 1) loose sand (Dr = 40%), 2) medium dense sand (Dr = 60%), 3) dense sand (Dr = 75%), and very

Table 1 Physical properties of Kumamoto silica sand (K7)

Property	Value	Unit
Specific gravity, G_s	2.63	-
Fine-grained soil	15.6	%
Unified Soil Classification System (USCS)	SM	-
Mean grain size, D_{50}	168.4	μm
Effective grain size, D_{10}	57.72	μm
Uniformity coefficient, C_u	1.64	-
Coefficient of gradation, C_c	1.07	-
Maximum density, ρ_{max}	1.571	g/cm^3
Minimum density, ρ_{min}	1.197	g/cm^3

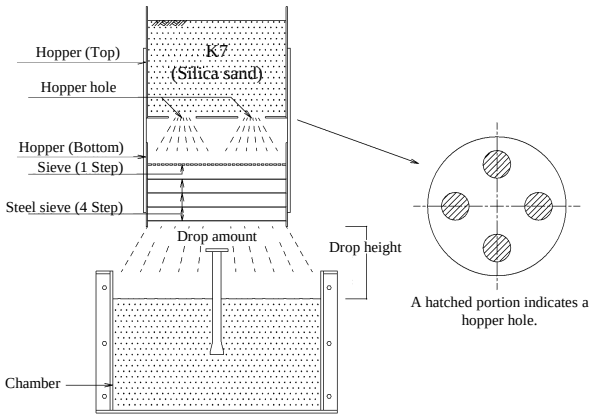

Fig. 6 Schematic diagram of hopper apparatus

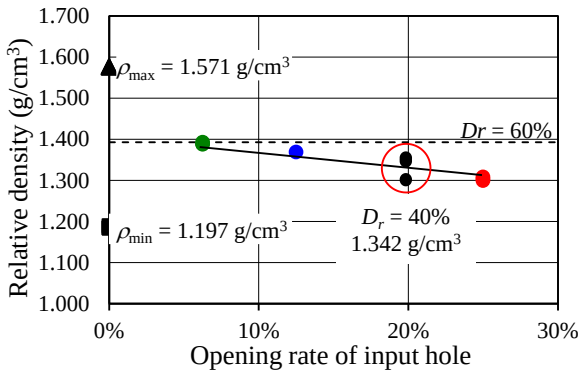

Fig. 7 Relative density (Dr) according to hopper hole size

dense sand (Dr = 85% and 95%). The relative density of the sand bed in the model experiment was calculated by determining the maximum and minimum densities. 1) The rain method and 2) compaction method were used to achieve the desired sand-bed density. Relative sand-bed densities of Dr = 40% and 60% were utilized in the rain method using the mobile hopper apparatus shown in Fig. 6. It can control the sand relative density by regulating the hole size at the bottom of the hopper suspension, and the hole opening rate was calibrated according to the density, as shown in Fig. 7. In the rain method procedure, the sand was dropped from a 1 m height from the hopper suspension hole. The compaction method was utilized to adjust the other sand-bed relative densities. The procedure involved

Table 2 Experimental test and numerical analysis conditions (small-scale model test and image analysis)

Chamber style	Relative density (%)	Pile tip inclination angle (θ_i, °)	Slenderness ratio (λ)	Etc
Circular	40, 60, 75, 85, 95	0, 12, 18		-
Half-circular	40, 75, 95	12, 30	3.33	Image analysis
FEM analysis	40, 75, 95	12		Soil Plus (v4.0)

Table 3 Tension uplift and compression speeds of the screw jack

Scale	Compress speed (mm/min)		Uplift speed (mm/min)	
2	3.86	3.84	-3.85	-3.87
2.7	5.45	5.44	-5.48	-5.45
3	6.44	6.45	-6.51	-6.52
4	9.06	9.08	-9.08	-9.09

calculating the weight of the sand at a height of 4 cm (one layer) in advance. Each layer was tamped using a rubber hammer to achieve the desired relative density. Four sand-bed layers were utilized to achieve the shallow-depth (16 cm) condition.

2.3 Model test set-up and instruments

Table 2 lists the experimental tests (small-scale model test and image analysis) and numerical analysis conditions. Fig. 8 shows the model apparatus, which consists of three parts: 1) the model chamber (circular chamber for the static tension uplift test and half-circular chamber for the image analysis), 2) loading device (screw jack for loading and operation panel for controlling the load and strain), and 3) measuring device (load cell, LVDT, and monitoring camera for image analysis). The model ground and model piles were prepared in three stages. First, the lower ground up to the end of the pile was prepared considering the relative density. Afterward, the lower ground was formed, and model piles were installed in the chamber. Thereafter, the upper ground was prepared using the same method as that for the lower ground. Friction is generated between the observation window and belled pile installed in the half-circular chamber. To prevent this, a 1 mm gap was created between the observation window and belled pile and filled with silicone grease to prevent spilling sand from the gap. A screw jack was used to apply strain-controlled loading. The maximum load of the screw jack is 10 kN, and the load and strain can be controlled using the operation panel. Table 3 lists the tension uplift and compression speeds of the screw jack. The tension uplift speed in this model test was set as 4 mm/min. A load cell and LVDT were installed in the model apparatus to measure the load and vertical displacement.

The maximum load of the load cell and LVDT displacement range were 2 t and 50 cm, respectively. The data were collected 200 times per minute to ensure test accuracy.

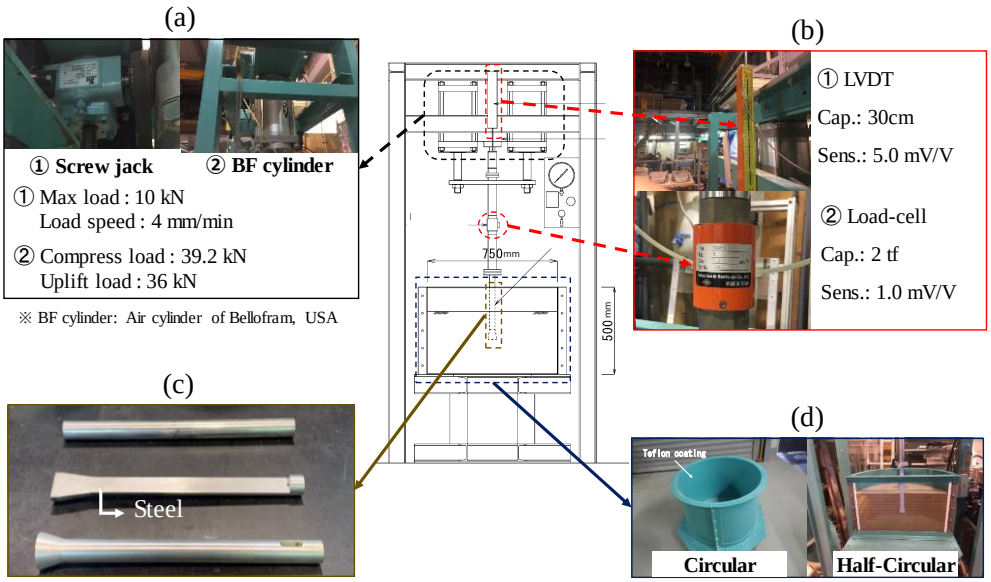

Fig. 8 Model apparatus: (a) loading system, (b) measuring apparatus, (c) model pile and (d) model chamber

(a) (b)

Fig. 9 Example of image analysis (Dr = 95% and θ_i = 12°): (a) before image analysis and (b) after image analysis

Table 4 Physical properties of the model ground used for FEM analysis (Soil Plus V.4.0)

γ (kN/m^3)	Dr (%)	E (MN/m^2)	ν	c (kN/m^2)	φ (°)	δ (°)	Ground model
12.9	40	75			35	23	
13.7	60	100			39	26	
14.3	75	125	0.3	0.1	41	27	*Elasto*-plastic
14.7	85	150			43	29	
15.2	95	200			45	30	

2.4 Image and FEM conditions

Images collected from the camera were used in the image analysis. After capturing an image, the initial image and the image corresponding to each displacement were compared based on 1 mm of uplift displacement in the monitoring data, and the deformed part was expressed as a change in color. Fig. 9 demonstrates the image analysis results obtained at Dr = 95% and θ_i = 12°.

Table 4 lists the physical properties of the model ground used for FEM analysis, which utilized Soil Plus (Version 4.0) software. The numerical model ground used is shown in Fig. 10. In the numerical model, a 2D axisymmetric model with a length of 375 mm and height of 500 mm from the center of the pile was used for FEM analysis. The elasticity modulus of the ground was 1/1000 of the initial

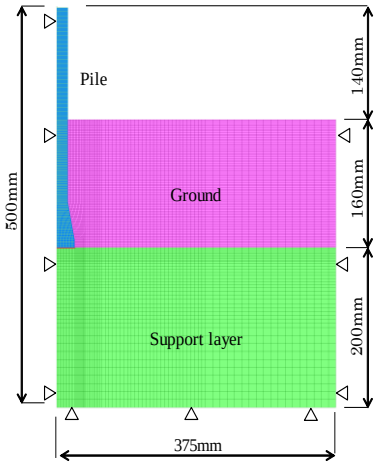

Fig. 10 Numerical model in Soil Plus v.4.0 program

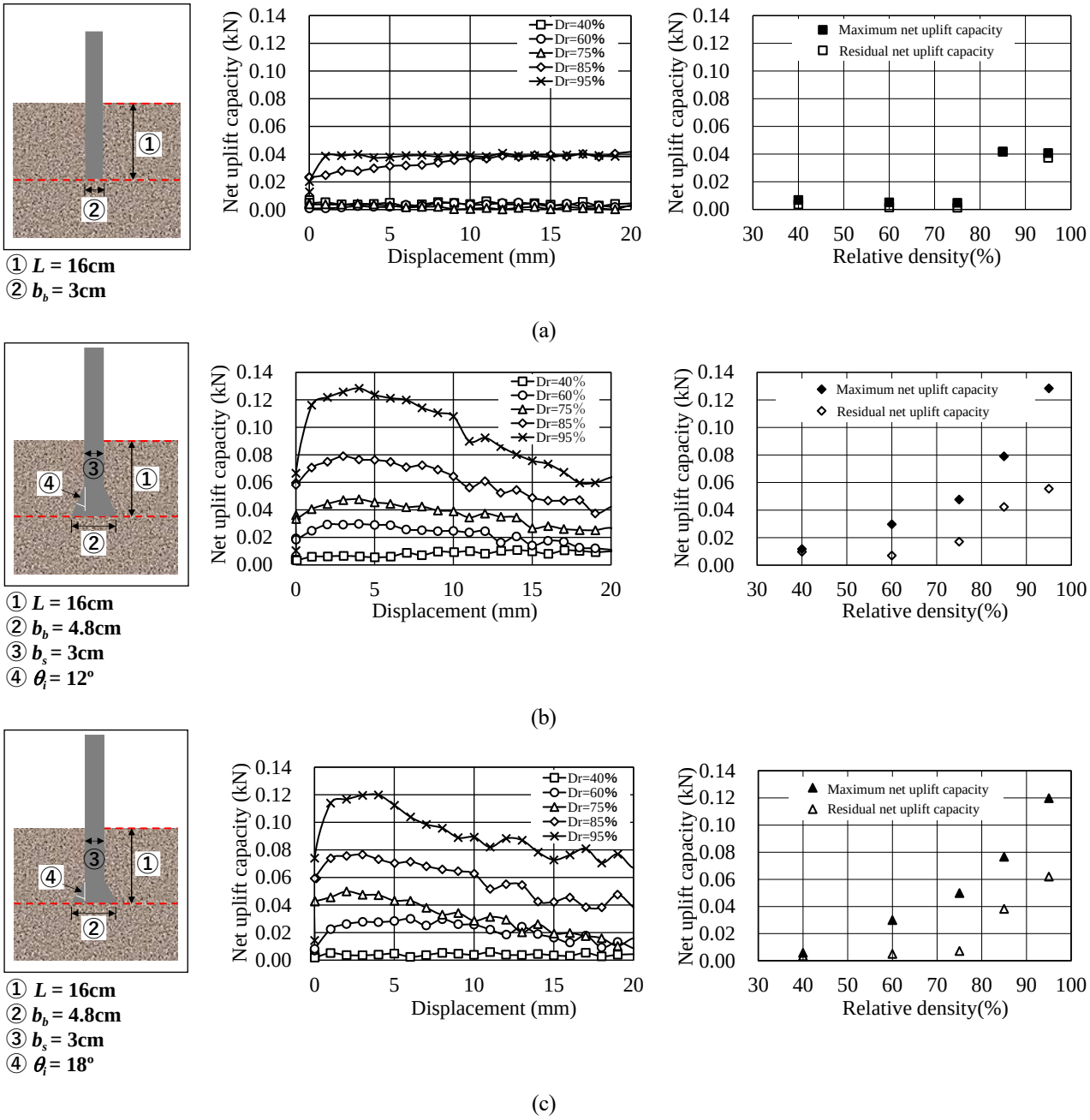

Fig. 11 Variation in the net uplift capacity and residual load with vertical displacement in belled piles with three pile-tip angles at a penetration depth of 16 cm: (a) conventional pile (θ_i = 0°), (b) belled pile (θ_i = 12°) and (c) belled pile (θ_i = 18°)

value and configured as an elastoplastic element based on the Mohr–Coulomb failure criterion. In addition, 2/3φ of the pile-soil skin friction angle(δ) was applied in the boundary condition between the pile and the ground (Terzaghi and Peck 1948), and the elasticity modulus between the ground support layer and belled pile was achieved via a 1/10000 reduction to simulate separation between the ground supporting layer and belled pile during the belled pile uplift.

In this analysis, the same conditions were applied to the ground soil and supporting layer. Here, because the belled pile is made of elastic material and is supported by a load device in the experimental model, its weight is neglected.

The boundary conditions were fixed in the vertical direction at the bottom part and laterally in the horizontal parts in the model. The uplift load was applied in 25 steps by applying a maximum uplift load of 0.5 kN to the pile head using the load control method.

3. Results and discussion

3.1 Laboratory model experiment

The results are collected from the instrumented belled

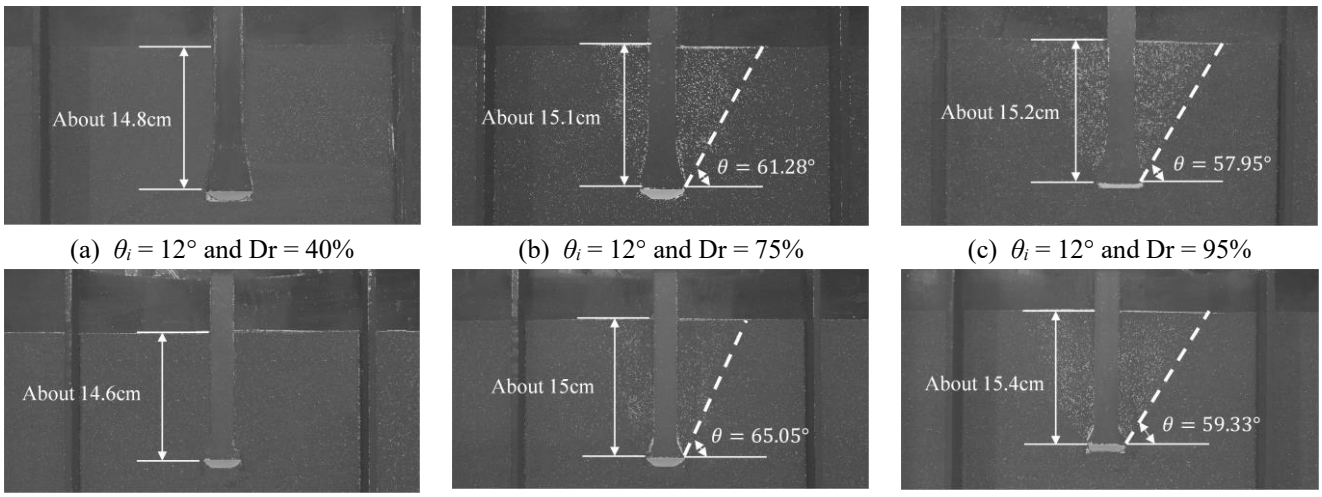

(a) θ_i = 12° and Dr = 40% (b) θ_i = 12° and Dr = 75% (c) θ_i = 12° and Dr = 95%

(d) θ_i = 30° and Dr = 40% (e) θ_i = 30° and Dr = 75% (f) θ_i = 30° and Dr = 95%

Fig. 12 Image analysis results for θ_i = 12° and 30° and Dr = 40%, 75%, and 95% at L= 16 cm

pile embedded in loose, medium, and dense sand during a laboratory model experiment. The variation in the net uplift capacity and residual load with vertical displacement in belled piles with three pile-tip angles at a penetration depth of 16 cm (L = 16 cm) is shown in Fig. 11. The net uplift capacity is obtained by subtracting the weight of the pile from the measured uplift load. The residual load was measured to analyze the uplift load characteristics of conventional and belled piles beyond the maximum uplift load. The residual load was measured up to a vertical displacement of 40 mm. Fig. 11(a) shows the net uplift capacity and residual load of a conventional pile (θ_i = 0°). The net uplift capacity was approximately 0.01 kN at a relative density of less than 75%. However, when the relative density exceeded 85%, the net uplift capacity was approximately 0.04 kN, which was approximately four times higher. In addition, the net uplift capacity and residual load values in all experimental results were similar for different relative densities. When the relative density of sand is less than 75%, the net uplift capacity is a result of the friction between the pile skin and ground, whereas when the relative density of sand exceeds 85%, the net uplift capacity is dependent on failure surface formation. This result is similar to that of a previous study that reported that failure surfaces are dependent on the relative density (Hong and Chim 2015).

Figs. 11(b) and 11(c) display the net uplift capacity and residual resistance of the belled piles (θ_i = 12° and 18°). The peak net uplift capacity cannot be measured at a relative density of 40% in loose sand. This phenomenon is due to fact that when a constant load at constant displacement is applied in very loose sand ground with a relative density of 40%, the sand ground is only compressed. Therefore, the resistance to the uplift capacity is not sufficiently expressed. However, the peak value of the net uplift capacity of the belled pile was confirmed in relative densities exceeding 60%. This is attributable to the effect of friction between the pile skin and ground and that of the belled pile-tip shape. Furthermore, marked differences in the residual strength between conventional and belled piles were observed in the experimental results, except at a density of 40%. For conventional piles, the peak uplift capacity was slightly higher than the residual strength, and this behavior was observed regardless of the relative density. However, in the belled pile, the difference between the peak net uplift capacity and residual load was evident beyond a relative density of 60%, and each value increased with an increase in the relative density. This is attributable to the resistance of the belled pile being higher than that of a conventional pile owing to the shape of the belled pile tip despite the peak uplift capacity being achieved.

3.2 Image analysis

In this study, image analysis was performed by monitoring the model experiment to determine the failure surface of the belled pile. Fig. 12 shows the image analysis results for θ_i = 12° and 30° and Dr = 40%, 75%, and 95% at L = 16 cm. The image analysis reveals that failure surfaces were not present at a relative density of 40% for both belled piles. However, they were clearly identified at relative densities of 75% and 95%. In both belled piles, the failure surfaces were widely distributed at a relative density of 95%, and the maximum failure surface was within 10 mm of the uplift displacement. In addition, the failure surface of the belled pile with θ_i = 12° was slightly wider than that of the belled pile with θ_i = 30° (by 2° or 3°).

The shape of the failure surface was similar to that of the inverted truncated cone model observed in previous studies. Therefore, the failure surface of the belled piles had a markedly wider surface under a high relative density and wide pile-tip area. Therefore, the resistance area of the belled shape and relative density of sand are more important parameters affecting the shape of the failure surface than the uplift capacity. In the image analysis for a conventional anchor plate conducted by Liu *et al*. (2012) loose sand exhibited volume shrinkage in the ground near the anchor

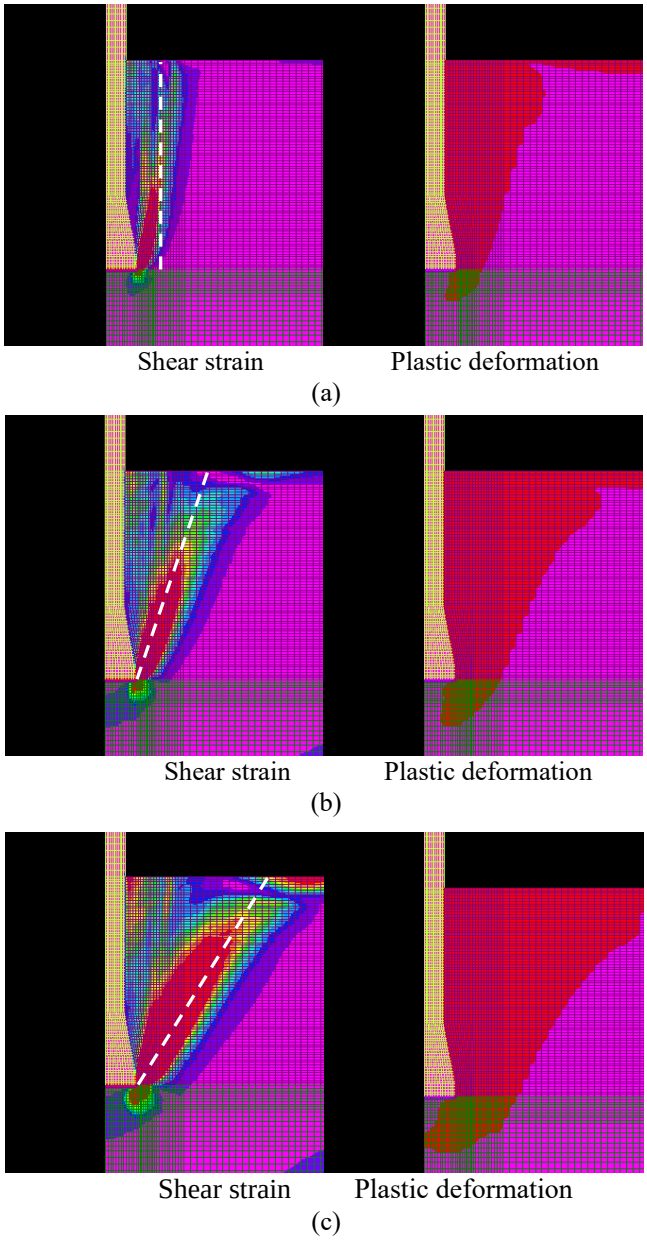

Fig. 13 The results of 2D FEM analysis after the uplift load of belled pile: (a) Dr = 40%, (b) Dr = 75% and (c) Dr = 95%

plate, whereas the dense sand exhibited volume expansion in the ground near the anchor plate. This trend is similar to that observed in the image analysis conducted in this study.

3.3 FEM analysis

The main purpose of the numerical analysis in this study was to investigate the formation of the failure surface and the failure angle according to the shape of the belled angle and soil density. The failure surface and failure angle from the belled pile-tip are very critical parameters for predicting the uplift capacity of belled piles. In this study, a new model to predict the uplift capacity of belled piles was proposed based on these parameters. Therefore, to derive accurate results of numerical analysis, FEM analysis was performed by applying the uplift load in 25 steps considering the results of the model experiment (uplift capacity: maximum 12.5 kN). Here, to confirm the change in the failure surface according to the uplift load, the change in maximum shear strain and plastic strain from the FEM analysis were used. Fig. 13 shows the results of 2D FEM analysis after the uplift load was reached. The maximum shear strain and plastic conditions were analyzed for a belled pile-tip angle of 12°. Accordingly, the maximum shear strain and plastic deformation were partially confirmed on the surface of the belled pile at a relative density of 40%. However, at relative densities of 75% and 95%, the range of shear strain and plastic deformation exhibited an inverted truncated cone model similar to that observed in the image analysis. In addition, the plastic deformation at a relative density of 95% was wider than that at a relative density of 75%. The maximum shear strain at relative densities of 75% and 95% corresponded to tip angles of 63.5° and 57.5°, respectively.

The difference in angles with these relative densities was approximately 5°. These results imply that the failure angle and size of the failure surface are determined by the relative density and belled pile-tip angle. Therefore, the FEM analysis corroborates the image analysis, thereby validating the boundary conditions and parameters applied in this study.

4. Predictive model for uplift capacity of belled pile

A predictive model for the uplift capacity of a belled pile was developed considering the effects of the belled pile-tip angle and relative density. The shape of the failure surface was determined by the image and FEM analyses of the belled pile-tip angles. In addition, a density coefficient, κ, was proposed to take into account the effect of the relative density on the ground conditions. The limit equilibrium equation for conventional piles was applied to calculate the uplift capacity of the belled pile in the failure surface.

4.1 Laboratory model experiment

The image and FEM analyses revealed that the failure surface was linearly formed from the ground surface to the tip of the model pile with a constant failure angle for both bell-shaped piles. The shape of this failure surface resembles the inverted truncated cone model from previous studies for conventional piles, belled piles, anchor plates, and screw piles among others, for shallow foundations (Ghaly *et al*. 1991, Ilamparuthi *et al*. 2002, Shanker *et al*. 2007). It was previously reported that the failure angle at the failure surface generated at the uplift capacity was determined by soil parameters such as adhesion, dilatancy angle, and internal friction angle (Sutherland 1965, Meyerhof 1968, Vermeer and Levacher 1985, Murray and Geddes 1987, Shanker *et al*. 2007). However, the application to the uplift capacity of a belled pile was limited because the effects of the belled pile-tip shape and pile-soil friction were not considered. Hence, this study proposed a

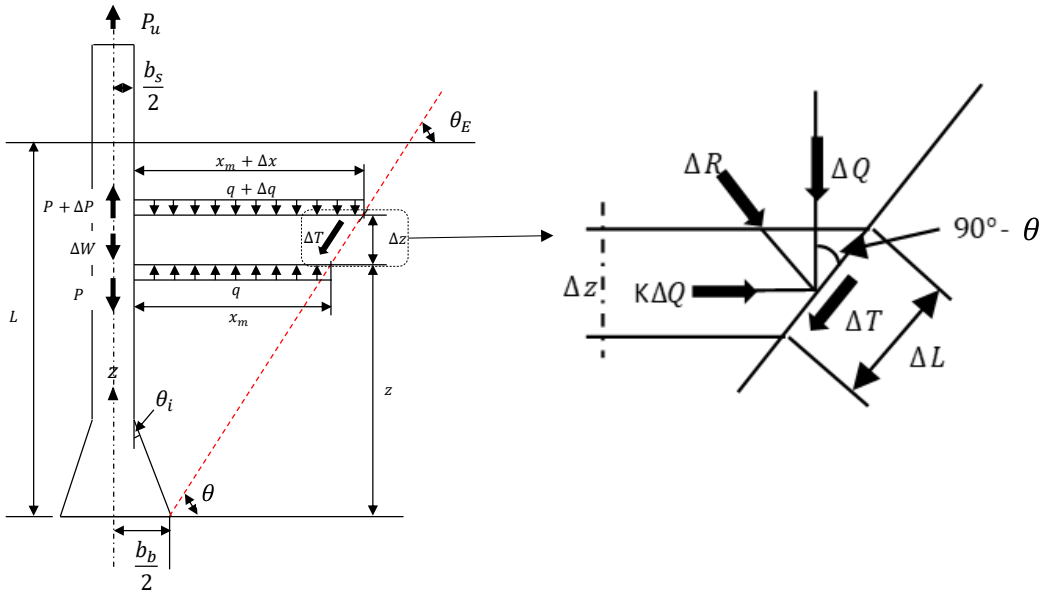

Fig. 14 The free-body diagram of circular disc wedge for applying the uplift resistance of belled pile

novel method of determining the failure angle of the failure surface while considering the belled pile-tip angle and relative as given in Eq. (1)

$$\theta = \left(90° - \frac{\psi}{2} - \theta_i\right) \tag{1}$$

where θ, θ_i, and ψ represent the failure, belled, and dilatancy angles (φ / 2°, φ - 30°). In this equation, the failure angle is defined as the sum of the failure angle of a conventional pile, as proposed by Shanker *et al*. (2007) and the belled pile-tip angle (θ_i). In addition, to consider the change in the net uplift capacity and failure angle with relative density observed in the image and FEM analyses, a new relative density coefficient is proposed in Eq. (2).

$$\kappa = (1 - \frac{Dr}{100} + 0.7) \tag{2}$$

where κ is the relative density coefficient. κ accounts for the tendency of the maximum net uplift capacity to increase more at a relative density of 70%. Finally, the failure angle can be determined using Eq. (3).

$$\theta = \kappa\left(90° - \frac{\psi}{2} - \theta_i\right) \tag{3}$$

4.2 Development of predictive uplift capacity model

In this study, a predictive model for the uplift capacity of belled pile for shallow foundations was proposed based on the observed failure angle, and failure surface and limit equilibrium equation for a conventional pile proposed by Chattopadhyay and Pise (1986). The predictive uplift capacity model for a conventional pile calculates the failure surface by considering the relationship between the pile-soil friction angle and internal friction angle of the soil. This model calculates the uplift capacity by calculating the soil weight inside the failure surface at a certain height and the shear force of the failure surface. Here, the limit equilibrium equation was used to efficiently calculate the weight of the soil within the failure surface for a specific height and the shear force of the failure surface. Hence, the limit equilibrium equation proposed by Chattopadhyay and Pise (1986) was introduced to efficiently calculate the proposed failure surface. To apply the limit equilibrium equation to the belled pile, three assumptions were made:

1. The maximum uplift capacity has occurred at the maximum failure surface.
2. The maximum uplift capacity for a belled pile is formed when the failure surface is maximal, and the internal friction angle and pile-skin friction angle are the same ($\delta = \varphi$).
3. The lateral earth pressure generated within the wedge plane at a given height is assumed to be $K = (1 - \sin\delta)(\tan\delta / \tan\varphi)$ and $\delta = \varphi$ under the maximum uplift capacity; thus, the lateral earth pressure can be assumed to be $K = (1\text{-}\sin\varphi)$.

Fig. 14 shows a free-body diagram of the circular disc wedge used for applying uplift resistance to the bell pile. The limit equilibrium equation can be obtained from the relationship between the mobilized shear strength of the soil along the failure surface and the uplift force from the weights of the soil and pile (Chattopadhyay and Pise 1986).

This limit equilibrium equation assumes a circular disk wedge of prescribed thickness (Δz) at the prescribed height (z) from the pile-tip between the axisymmetric failure surface and the belled pile. This assumption is applicable to calculating the reaction force of the failure surface against the weight (ΔW) of the soil and shear resistance (ΔT) on Δz. Considering the previous limit equilibrium equation, the predictive model of the bell pile can be derived as follows:

The mobilized shear resistance (ΔT) along the failure surface of length (ΔL) under the limiting condition is

$$\Delta T = \Delta R tan\varphi \tag{4}$$

where ΔR = Normal force acting on the failure of wedge

$$\Delta R = \Delta Q cos\theta + K_0 \Delta Q sin\theta \tag{5}$$

$$\text{where } \Delta Q = \gamma_d \left(L - z - \frac{\Delta z}{2}\right) \Delta L \tag{6}$$

Borrowing from Chattopadhyay and Pise (1986), the coefficient of the lateral earth pressure within the wedge is taken as

$$K = (1 - sin\varphi)(tan\delta / tan\varphi) \tag{7-1}$$

$$\delta = \varphi \ \rightarrow K = K_0 = (1 - sin\varphi) \tag{7-2}$$

Substituting Eq. (5) into Eq. (6), we get

$$\Delta R = \gamma_d \left(L - z - \frac{\Delta z}{2}\right)(cos\theta + K_0 sin\theta)\Delta L = \gamma_d \left(L - z - \frac{\Delta z}{2}\right)(cos\theta + K_0 sin\theta)\frac{\Delta z}{sin\theta} \tag{8}$$

Substituting Eq. (4) into Eq. (8)

$$\Delta T = \gamma_d \left(L - z - \frac{\Delta z}{2}\right)(cos\theta + K_0 sin\theta)\frac{\Delta z tan\varphi}{sin\theta} \tag{9}$$

Considering the vertical equilibrium of the circular disc wedge and assuming that the weight of the pile of length Δz is equal to the weight of the soil corresponding to the volume occupied by the pile for the length Δz

$$(P + \Delta P) - P + q\pi \left(x_m + \frac{b_b}{2}\right)^2 - (q + \Delta q)\pi \left(x_m + \frac{b_b}{2} + \Delta x\right)^2 - \Delta W - 2\pi \left(x_m + \frac{b_b}{2} + \frac{\Delta x}{2}\right)\Delta T sin\theta = 0 \tag{10}$$

where Δx denotes the horizontal increment on the failure surface with Δz.
Substituting Eqs. (9) into (10), we get

$$\frac{\Delta P}{\Delta z} = q\frac{\Delta x}{\Delta z}\left(2 \times \left(x_m + \frac{b_b}{2}\right) + \Delta x\right) + \frac{\Delta q}{\Delta z}\left(x_m + \frac{b_b}{2} + \Delta x\right)^2 + 2\pi\gamma_d \left(x_m + \frac{b_b}{2} + \frac{\Delta x}{2}\right)^2 + 2\pi \left(x_m + \frac{b_b}{2} + \frac{\Delta x}{2}\right)\gamma_d \left(L - \mathrm{z} - \frac{\Delta z}{2}\right)(cos\theta + K_0 sin\theta)tan\varphi \tag{11}$$

After simplification

$$\frac{dP}{dz} = 2\pi \left(x_m + \frac{b_b}{2}\right) q \frac{dx}{dz} + 2\pi \left(x_m + \frac{b_b}{2}\right)\gamma_d (L - \mathrm{z})(cos\theta + Ksin\theta)tan\varphi \tag{12}$$

Because $q = \gamma_d (L - z)$, $cot\,\theta = \frac{dx}{dz}$, and Eq. (12) can be rewritten as

$$dP = 2\gamma_d \pi \left(x_m + \frac{b_b}{2}\right)(L - z)[cot\,\theta + (cos\theta + K_0 sin\theta)tan\varphi]dz \tag{13}$$

Therefore, the uplift capacity P_u of the belled pile for shear failure is given by

$$P_u = \int_0^L 2\gamma_d \left(x_m + \frac{b_b}{2}\right)(L - z)\,[cot\,\theta + (cos\theta + K_0 sin\theta)tan\varphi]dz = \gamma_d \left(x_m + \frac{b_b}{2}\right) L^2 [cot\,\theta\,(cos\theta + K_0 sin\theta)tan\varphi] \tag{14}$$

where the net uplift capacity Pu(net) is expressed in Eq. (15).

$$\therefore P_{u(net)} = P_u - W_{pile} \tag{15}$$

5. Validation of proposed predictive model

5.1 Previous predictive models for determining the uplift capacity

In this section, the proposed model was compared and analyzed with previous predictive models for determining the uplift capacity in a conventional pile, belled pile, and anchor plate system to validate the proposed predictive model.

5.1.1 Conventional pile

Standard model

The standard model estimates the net uplift capacity assuming that a cylindrical failure surface is formed around the pile and can be expressed as

$$P_{u(net)} = \pi/2 K_s b_b \gamma_d L^2 tan\delta \tag{16}$$

where K_s is the lateral earth pressure, b_b is the diameter of the pile tip, γ_d is the dry unit weight, and δ is the pile-soil friction angle. The main parameters in this model are the pile-soil friction angle and the lateral earth pressure. In addition, Levacher and Sieffert (1984) reported that K_s can determined by 1-sinφ.

Truncated cone model

The truncated-cone model is generally used in the field. It assumes that the shape of the failure surface is formed linearly to the ground along the failure surface angle from the pile tip. This shape of the failure surface corresponds to the previously proposed inverted truncated-cone model. Therefore, the uplift capacity is calculated using the weight of the soil in the assumed failure surface and the internal friction angle as follows

$$P_{u(net)} = \pi/3 L^3 \, tan^2 \frac{\varphi}{2} \gamma_d \tag{17}$$

5.1.2 Belled pile and anchor plate

The theory of the uplift capacity for belled piles was previously established (Balla 1961, Downs and Chieurzzi 1966, Meyerhof and Adams 1968, Ovesen 1981). In previous studies, the predictive uplift capacity model of belled piles considered factors such as the pile-soil skin friction, shear stress at the failure surface, weight of soil inside the failure surface, and the diameter of the belled pile tip.

Downs and Chieurzzi (1966)

Downs and Chieruzzi (1966) proposed a predictive model for the uplift capacity based on field tests on belled

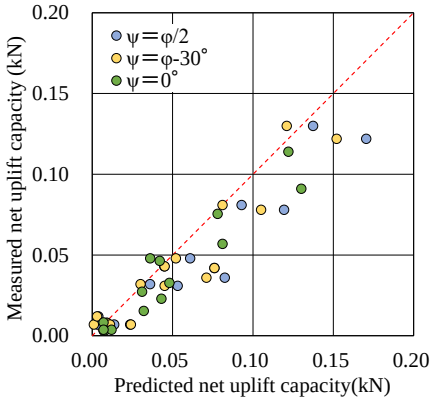

Fig. 15 The comparison for results of predictive model calculated by two methods of dilatancy angle (ψ)

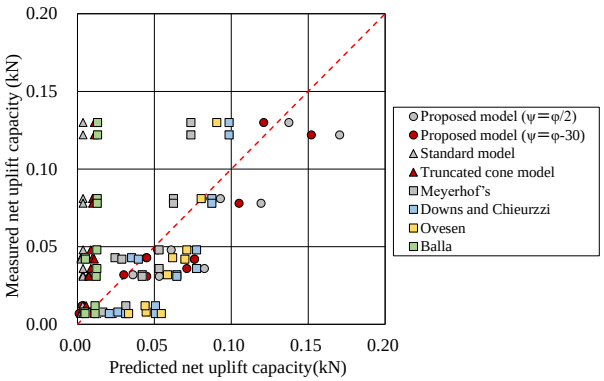

Fig. 16 The comparisons for result of laboratory model test calculated by the proposed predictive model and previous models

piles. In this model, the failure surface is assumed to be an inverted cone, and the uplift capacity is calculated from the sum of the weight of the soil in the failure surface and the weight of the pile.

$$P_u = \gamma_d A_b L\{1 + 2(L/B)tan\varphi + (4/3(L/B)^2\, tan^2\,\varphi + (b_s/b_b)\} \quad (18)$$

where b_s is the center diameter of the belled pile.

Meyerhof and Adams (1968)

Meyerhof and Adams (1968) proposed a model to predict the net uplift capacity of a belled pile. In their study, a pyramid-shaped slip surface similar to a shallow anchor is assumed for calculating the net uplift resistance of the belled pile, and its model can be expressed as follows

$$P_u = \gamma_d A_b L(2\left(\frac{L}{b_b}\right)K_u tan\varphi\left[m\left(\frac{L}{b_b}\right)+1\right]+1) \quad (19)$$

where A_b is the area of the belled pile tip, b_b is the diameter of the belled pile tip, K_u is the horizontal earth pressure coefficient, and m is the shape factor for the internal friction angle.

Ovesen (1981)

Ovesen (1981) derived an empirical model for the uplift capacity for a horizontal anchor plate using a centrifugal model test.

$$P_u = \gamma_d A_b L\{1 + (4.32^* tan\varphi - 1.58)(L/B_e)^{1.5}\} \quad (20)$$

where B_e is the coefficient for the effect of the diameter of the belled pile tip and $B_e = (\pi B^2/4)^{1/2}$.

Balla (1961)

Balla (1961) derived an empirical model of the uplift capacity for a mushroom foundation assuming that the failure surface is formed by the tangential-curve slip surface based on a laboratory model test, and its model can be expressed as follows

$$P_u = \gamma_d A_b L\{(F_1 + F_3)(4/\pi)(H/B)^2\} \quad (21)$$

where F_1 and F_3 are functions of the peak friction angles φ' and γ_d obtained from the chart provided by Balla (1961).

F1 and F3 have the following relationship

$$F_1 + F_3 = -0.0171\left(\frac{L}{b_b}\right)^3 + 0.3057\left(\frac{L}{b_b}\right)^2 - 1.7937\left(\frac{L}{b_b}\right) + 4.0389 \quad (22)$$

5.2 Validation and verification of proposed predictive model

Fig. 15 and Table 5 present the comparison of the results of the predictive model calculated using the two methods of calculating the dilatancy angle. The dilatancy angle is an important parameter in the proposed model for calculating the uplift capacity of a belled pile. In this study, the dilatancy angles were calculated using two methods for $\psi = \varphi / 2$ and $\psi = \varphi - 30$ considering the internal friction angle (Dickin and Leung 1990).

In addition, to evaluate the accuracy of the predictive models, an error rate (ε) was introduced using Eq. (23).

$$\varepsilon\,(\%) = \left|\frac{P_{u(predictive\ model)} - P_{u(experiment)}}{(P_u)_{experiment}}\right| \times 100 \quad (23)$$

The calculated dilatancy angles were applied to the proposed predictive model. The uplift capacity values obtained from the predictive model using $\psi = \varphi - 30$ well fitted the uplift capacity values obtained from the laboratory model test. The results for each dilatancy angle at a relative density of 40% show a high ε value because of the high compressibility of loose sand at a low relative density. Except at a relative density of 40%, ε was low: it was 28.6% and 23.2% at $\psi = \varphi / 2$ and $\psi = \varphi - 30$, respectively.

Fig. 16 and Table 6 compare the results from the laboratory model test calculated using the proposed predictive model and previous models. The comparison results confirmed that the standard model and truncated-cone model for calculating the uplift capacity of a conventional pile has a very high ε value: from 105.4% to 3532.3%. This is attributable to using the conventional pile model to calculate the uplift capacity. In addition, the result calculated by Balla's model to calculate the uplift capacity

Table 5 Comparison of the results of the predictive model calculated using the two methods of calculating the dilatancy angle

Belled angle	Relative density	Unit weight	Internal friction angle	The proposed model						Experiment
θ_i (˚)	(%)	(kN/m^3)	φ (°)	P_u(kN)	ε (%)	P_u(kN)	ε (%)	P_u(kN)	ε (%)	P_u (kN)
	40	13.13	35	0.0032	115.7	0.003	115.7	0.001	600.0	0.007
	65	13.88	39	0.0035	131.3	0.009	12.6	0.009	11.1	0.008
0	75	14.44	41	0.0083	15.6	0.024	70.3	0.024	70.8	0.007
	85	14.81	43	0.0230	86.9	0.045	3.9	0.045	4.4	0.043
	95	15.19	45	0.0465	9.6	0.076	44.7	0.076	44.7	0.042
	40	13.13	35	0.0038	218.7	0.004	218.7	0.003	300.0	0.012
	65	13.88	39	0.0154	107.3	0.036	11.1	0.03	6.7	0.032
12	75	14.44	41	0.0328	46.5	0.061	21.1	0.052	7.7	0.048
	85	14.81	43	0.0569	42.3	0.093	12.8	0.081	0.0	0.081
	95	15.19	45	0.0911	42.7	0.137	5.4	0.121	7.4	0.13
	40	13.13	35	0.0038	85.9	0.014	48.6	0.011	36.4	0.007
	65	13.88	39	0.0273	13.4	0.053	41.6	0.045	31.1	0.031
18	75	14.44	41	0.0480	24.9	0.082	56.3	0.071	49.3	0.036
	85	14.81	43	0.0755	3.2	0.119	34.6	0.105	25.7	0.078
	95	15.19	45	0.1140	7.0	0.170	28.4	0.152	19.7	0.122

Table 6 Comparison for the results from the laboratory model test calculated using the proposed predictive model and previous models Comparison

Belled angle	Relative density	Unit weight	Internal friction angle	Standard model		Truncated cone model		Meyerhof's model		Downs and Chieurzzi		Ovesen		Balla		The proposed model				Experiment
																$\psi = \varphi/2$		$\psi = \varphi$-30°		
θ_i(°)	(%)	(kN/m^3)	φ (°)	P_u (kN)	ε (%)	P_u (kN)	ε (%)	P_u (kN)	ε (%)	P_u (kN)	ε (%)	P_u (kN)	ε (%)	P_u (kN)	ε (%)	P_u (kN)	ε (%)	P_u (kN)	ε (%)	P_u (kN)
	40	13.13	35	0.002	228.7	0.006	25.0	0.012	42.8	0.021	66.2	0.033	78.9	0.004	57.6	0.003	115.7	0.001	600.0	0.007
	65	13.88	39	0.002	262.5	0.007	10.2	0.016	51.2	0.026	69.4	0.045	82.1	0.005	69.8	0.009	12.6	0.009	11.1	0.008
0	75	14.44	41	0.002	213.0	0.009	19.7	0.021	66.2	0.031	77.6	0.054	87.1	0.005	43.3	0.024	70.3	0.024	70.8	0.007
	85	14.81	43	0.002	1817.7	0.010	339.0	0.024	76.6	0.035	22.5	0.062	30.4	0.005	761.9	0.045	3.9	0.045	4.4	0.043
	95	15.19	45	0.002	1777.6	0.011	282.9	0.029	45.9	0.040	6.3	0.070	39.8	0.005	726.8	0.076	44.7	0.076	44.7	0.042
	40	13.13	35	0.003	252.2	0.006	114.3	0.031	61.7	0.051	76.3	0.044	72.6	0.011	5.6	0.004	218.7	0.003	300.0	0.012
	65	13.88	39	0.004	806.3	0.007	340.8	0.042	23.8	0.065	50.4	0.058	45.2	0.012	165.3	0.036	11.1	0.03	6.7	0.032
12	75	14.44	41	0.004	1241.4	0.009	450.8	0.053	9.4	0.077	37.9	0.071	32.4	0.013	283.7	0.061	21.1	0.052	7.7	0.048
	85	14.81	43	0.004	2157.7	0.010	727.0	0.062	30.0	0.087	7.2	0.080	0.8	0.013	534.2	0.093	12.8	0.081	0.0	0.081
	95	15.19	45	0.004	3532.3	0.011	1085.1	0.074	76.4	0.098	32.0	0.090	43.7	0.013	899.7	0.137	5.4	0.121	7.4	0.13
	40	13.13	35	0.003	105.4	0.006	25.0	0.031	77.7	0.051	86.2	0.044	84.0	0.011	38.4	0.014	48.6	0.011	36.4	0.007
	65	13.88	39	0.004	777.9	0.007	327.1	0.042	26.2	0.065	52.0	0.058	46.9	0.012	157.0	0.053	41.6	0.045	31.1	0.031
18	75	14.44	41	0.004	906.0	0.009	313.1	0.053	32.1	0.077	53.5	0.071	49.3	0.013	187.8	0.082	56.3	0.071	49.3	0.036
	85	14.81	43	0.004	2074.1	0.010	696.3	0.062	25.2	0.087	10.6	0.080	2.9	0.013	510.7	0.119	34.6	0.105	25.7	0.078
	95	15.19	45	0.004	3308.8	0.011	1012.1	0.074	65.5	0.098	23.9	0.090	34.9	0.013	838.2	0.170	28.4	0.152	19.7	0.122

for the mushroom foundation yields a very high ε of 352.0% even though the mushroom foundation is similar to the belled pile and anchor plate. The value is lower than that of conventional piles because the shape effect of the mushroom foundation tip is minor because the foundation is buried at a shallow depth. The ε value for the belled pile and anchor plate are 47.4%, 44.8%, and 48.7% for the other models. These models exhibited a lower ε than the conventional pile model.

Consequently, the previous models (Standard and Truncated cone models) were proposed for conventional piles (straight pile) and these models did not consider the effect of belled pile-tip shape. In addition, Bella's model for the belled pile and anchor plate only considers the diameter

of the belled pile-tip, not considering the effect of the belled pile-tip shape. Therefore, this model does not include the effect of uplift capacity on the belled pile-tip shape. For this reason, the previously proposed models are not suitable for estimating the uplift capacity of belled piles.

6. Conclusions

Laboratory model experiments were conducted to measure the uplift capacity of a belled pile buried a shallow depth considering the effects of the relative density of sand and belled pile-tip angle. Image and FEM analyses were used. From the result, a predictive model for the uplift capacity of a belled pile was proposed and compared with previous models to validate the applicability of the proposed model. The following conclusions can be drawn:

• The reduction of natural frequency depends on the crack depth and crack location In the laboratory model experiment, no significant difference in the net uplift capacity and the residual resistance between the conventional pile and belled pile is observed when the relative density is below 40%. The net uplift capacity and residual resistance of the belled pile were higher than those of a conventional pile with increasing relative density. In addition, the net uplift capacity changed with the belled pile-tip angle. Thus, the resistance area of the belled pile is a more dominant factor than the pile-tip angle in the development of the uplift capacity of a belled pile.

• Failure surfaces were not observed at a relative density of 40% for all piles in the image analysis. However, for relative densities of 75% and 90%, the shape of the failure surface was clearly identified as an inverted truncated cone. In addition, the shape of the failure surface of the belled pile with a pile-tip angle of 12° was slightly wider by 2° or 3° than that of the belled pile with a tip angle of 30°. In addition, the shape of the failure surface in the FEM analysis resembled the inverted truncated cone from the image analysis. Thus, the shape and size of the failure surface of the belled pile depend on the relative density and belled pile-tip angle.

• A predictive model for the net uplift capacity of belled pile was proposed considering the effects of the relative density and belled pile-tip angle based on the limit equilibrium equation. The proposed model showed good agreement with the results obtained from the laboratory model experiment and has satisfactory applicability better than previous models.

Acknowledgments

This work was supported by the National Research Foundation of Korea (NRF) grant funded by the Korea government (MSIT) (No. 2021R1C1C2004070) and the research funds from Gwangju University in 2023.

References

Balla, A. (1961), "The resistance to breaking-out of mushroom foundations for pylons", *Proceedings of the 5th. Int. Conf. on SMFE*, Paris, France, July.

Emirler, B., Tolun, M. and Laman, M. (2016), "Experimental investigation of the uplift capacity of group anchor plates embedded in sand", *Geomech. Eng.*, **11**(5), 691-711. https://doi.org/10.12989/gae.2016.11.5.691.

Ghaly, A., Hanna, A. and Hanna, M. (1991), "Installation torque of screw anchors in dry sand", *Soils Found.*, **31**(2), 77-92. https://doi.org/10.3208/sandf1972.31.277.

Chatani, F., Suzuki, N., Nishimura, K. and Wada, Y. (2008), "Static axial reciprocal and tensile load tests of single cast-in-place concrete nodular piles, Part 5", *In Annual Meeting of Architectural Istitute of Japan*, Japan.

Chattopadhyay, B.C. and Pise, P.J. (1986), "Uplift capacity of piles in sand", *J. Geotech. Eng.*, **112**(9), 888-904. https://doi.org/10.1061/(ASCE)0733-9410(1986)112:9(888).

Clemence, S.P. and Veesaert, C.J. (1977), "Dynamic Pullout Resistance of Anchors in Sand", *Proceedings of the Int Symp on Soil Struct Interaction*, Roorkee, India, January.

Dash, B.K. and Pise, P.J. (2003), "Effect of compressive load on uplift capacity of model piles", *J. Geotech. Geoenviron. Eng.*, **129**(11), 987-992. https://doi.org/10.1061/(ASCE)1090-0241(2003)129:11(987).

Deb, T. and Pal, S.K. (2019), "Study on the uplift behaviour and failure pattern of single belled anchor with 3D and 2D models in cohesionless soil bed", *Iran. J. Sci. Technol. Trans. Civ. Eng.*, **43**(3), 327-343. https://doi.org/10.1007/s40996-018-0144-x.

Deb, T. and Pal, S.K. (2019), "Comparison of uplift capacity and nonlinear failure surfaces of single-belled anchor in homogeneous and layered sand deposits", *Adv. Civ. Eng.*, **2019**, https://doi.org/10.1155/2019/4672615.

Dickin, E.A. and Leung, C.F. (1990), "Performance of piles with enlarged bases subject to uplift forces", *Can. Geotech. J.*, **27**(5), 546-556. https://doi.org/10.1139/t90-070.

Dickin, E.A. and Leung, C.F. (1992), "The influence of foundation geometry on the uplift behaviour of piles with enlarged bases", *Can. Geotech. J.*, **29**(3), 498-505. https://doi.org/10.1139/t92-054.

Downs, D.I. and Chieurzzi, R. (1966), "Transmission tower foundations", *J. Power Div.*, **92**(2), 91-114. https://doi.org/10.1061/JPWEAM.0000518.

Honda, T., Hirai, Y. and Sato, E. (2011), "Uplift capacity of belled and multi-belled piles in dense sand", *Soils Found*, **51**(3), 483-496. https://doi.org/10.3208/sandf.51.483.

Hong, W.P. and Chim, N. (2015), "Prediction of uplift capacity of a micropile embedded in soil", *KSCE J. Civ. Eng.*, **19**(1), 116–126. https://doi.org/10.1007/s12205-013-0357-2.

Keskin, M.S. (2015), "Model studies of uplift capacity behavior of square plate anchors in geogrid-reinforced sand", *Geomech. Eng.*, **8**(4), 595-613. https://doi.org/10.12989/gae.2015.8.4.595.

Khadilkar, B.S., Shinkre, P.R. and Karandikar, A.V. (1971), "Laboratory investigations of stress measurements in soils", *Indian Geotech. J.*, 53.

Kishida, H. (1963), "Stress distribution by model piles in sand", *Soils Found.*, **4**(1), 1-23. https://doi.org/10.3208/sandf1960.4.1.

Ilamparuthi, K. and Muthukrishnaiah, K. (1999), "Anchors in sand bed: delineation of rupture surface", *Ocean Eng.*, **26**(12), 1249-1273. https://doi.org/10.1016/S0029-8018(98)00034-1.

Ilamparuthi, K., Dickin, E.A. and Muthukrisnaiah, K. (2002), "Experimental investigation of the uplift behaviour of circular plate anchors embedded in sand", *Can. Geotech. J.*, **39**(3), 648-664. https://doi.org/10.1139/t02-005.

JGS 0560 (2020), Method for consolidated constant volume direct box shear test on soils, Japanese Geotechnical Society Standard, Japan.

JIS. A. 1224 (2009), Test method for minimum and maximum densities of sands, Japanese Industrial Standard, Japan.

Jinyuan Liu, P.E., Eng, P., Liu, M. and Zhu, Z. (2012), "Sand deformation around an uplift plate anchor", *J. Geotech. Geoenviron. Eng*., **138**(6), 728-737. https://doi.org/10.1061/(ASCE)GT.1943-5606.0000633.

Levacher, D.R. and Sieffert, J.G. (1984), "Tests on model tension piles", *J. Geotech. Eng.*, **110**(12), 1735-1748. https://doi.org/10.1061/(ASCE)0733-9410(1984)110:12(1735).

Lu, X.L., Qian, Z.Z. and Yang, W.Z. (2017), "Axial Uplift Behavior of Belled Piers in Sloping Ground", *Geotech. Test. J*., **40**(4), 505-510. https://doi.org/10.1520/GTJ20150202.

Majer, J. (1955), "Zur berechnung von zugfundamenten", *Osterreichische Bauzeitschrift*", **10**(5), 85-90.

Matsuo, M. (1967), "Study on the uplift resistance of footing (I)", *Soils Found.,* **7**(4), 1-37. https://doi.org/10.3208/sandf1960.7.41.

Matsuo, M. (1968), "Study on the uplift resistance of footing (II)", *Soils Found*., **8**(1), 18-48. https://doi.org/10.3208/sandf1960.8.18.

Meyerhof, G.G. (1959), "Compaction of sands and bearing capacity of piles", *J. Soil Mech. Found. Div.*, **85**(6), 1-29. https://doi.org/10.1061/JSFEAQ.0000231.

Meyerhof, G.G. and Adams, J.I. (1968), "The ultimate uplift capacity of foundations", *Can. Geotech. J.*, **5**(4), 225-244. https://doi.org/10.1139/t68-024.

Murray, E.J. and Geddes, J.D. (1987), "Uplift of anchor plates in sand", *J. Geotech. Eng*., **113**(3), 202-215.

Nazir, R., Moayedi, H., Pratikso, A. and Mosallanezhad, M. (2015), "The uplift load capacity of an enlarged base pier embedded in dry sand", *Arab. J. Geosci*., **8**(9), 7285-7296. https://doi.org/10.1007/s12517-014-1721-3.

Nguyen, A.D., Nguyen, V.T. and Kim, Y.S. (2023), "Finite element analysis on dynamic behavior of sheet pile quay wall dredged and improved seaside subsoil using cement deep mixing", *Int. J. Geoeng.*, **14**(1), 9. https://doi.org/10.1186/s40703-023-00186-x.

Niroumand, H. and Kassim, K.A. (2013), "A review on uplift response of symmetrical anchor plates embedded in reinforced sand", *Geomech. Eng*., **5**(3), 187-194. https://doi.org/10.12989/gae.2013.5.3.187.

Ovesen, N.K. (1981), "Centrifuge tests of uplift capacity of anchors", *Proceedings of the 10th. Int. Conf. on SMFE*, Stockholm, Sweden, June.

Perumalsamy, K. and Ranganathan, S. (2022), "Single pile in cohesionless soil in sloping ground under lateral loading", *Int. J. Geoeng.*, **13**(1), 8. https://doi.org/10.1186/s40703-022-00173-8.

Takagagi, T., Tsutsui, M., Katoh, K. and Shimatani, Y. (1995), "Experimental study on pulling resistance of cast-in-place belled pile,-Part 1", *In Annual Meeting of Architectural Institute of Japan.*, Japan.

Qian, Z., Lu, X. and Yang, W. (2019), "Comparative field tests on straight-sided and belled piers on sloping ground under combined uplift and lateral loads", *J. Geotech. Geoenviron. Eng*., **145**(12), 04018099. https://doi.org/10.1061/(ASCE)GT.1943-5606.0001991.

Qian, Z., Lu, X. and Yang, W. (2020), "Comparative lateral load field tests on straight-sided and belled piers in sloped ground", *Geotech. Eng.*, **173**(1), 70-80. https://doi.org/10.1680/jgeen.18.00151.

Robinsky, E.I. and Morrison, C.F. (1964), "Sand displacement and compaction around model friction piles", *Can. Geotech. J.*, **1**(2), 81-93. https://doi.org/10.1139/t64-002.

Schafer, M. and Madabhushi, S.P.G. (2020), "Uplift resistance of enlarged base pile foundations", *Indian Geotech. J*., **50**(3), 426-441. https://doi.org/10.1007/s40098-019-00369-3.

Shanker, K., Basudhar, P.K. and Patra, N.R. (2007), "Uplift capacity of single piles: predictions and performance", *Geotech. Geol. Eng.*, **25**(2), 151-161. https://doi.org/10.1007/s10706-006-9000-z.

Sutherland, H.B. (1965), "Model studies for shaft raising through cohesionless soils", *Proceedings of the 6th. Int. Conf. on SMFE*, Montreal, Canada, September.

Terzaghi, K. and Peck, R.B. (1948), Soil Mechanics in Engineering Practice, John Wiley and Sons, New York, NY, USA.

Vashishtha, H.R. and Sawant, V.A. (2021), "An experimental investigation for pullout response of a single granular pile anchor in clayey soil", *Int. J. Geoeng.*, **12**(35), 1-19. https://doi.org/10.1186/s40703-021-00162-3.

Vermeer, P.A. and Sutjiadi, W. (1985), "The uplift resistance of shallow embedded anchors", *Proceedings of the 11th. Int. Conf. on SMFE*, San Francisco, US, August.

Wang, Q., Ma, J., Xiao, Z., Chen, W. and Ji, Y. (2020), "Field test on uplift bearing capacity of rock-socketed belled piles", *KSCE J. Civ. Eng*., **24**(8), 2353-2363. https://doi.org/10.1007/s12205-020-2011-0.

IC

Notation

b_b = Tip diameter of the belled pile
b_s = Shaft diameter of the belled pile
δ = Pile-soil friction angle
Dr = Relative density
θ = Failure angle
θ_i = Belled angle
κ = Relative density coefficient
K = The coefficient of lateral earth pressure
K_0 = Earth pressure at rest
L = Pile penetration depth
P_u = Uplift capacity
$P_{u(Net)}$ = Net uplift capacity
ΔR = Reaction force
T = Shear stress at failure surface
ΔT = Shear force on differential volume inside failure surface
Q = Volume inside failure surface
ΔQ = Differential volume inside failure surface
W = Pile weight
ΔW = Weight of the soil within the failure surface
γ_d = Dry unit weight
φ = Internal friction angle
ψ = Dilatancy angle ($\psi = \varphi / 2°$; $\psi = \varphi - 30°$)
x_m = Horizontal distance from the pile to the failure surface